JOURNAL OF AIRCRAFT
Vol. 48, No. 4, July–August 2011

Wake Effects of Free-Wake Model on Aeroelastic Behavior of Hovering Rotors

Seung-Jae Yoo,* Min-Soo Jeong,* and In Lee†
Korea Advanced Institute of Science and Technology, Daejeon 305-701, Republic of Korea

DOI: 10.2514/1.C031172

The wake effects on aeroelastic deflections and aerodynamics for the isotropic and composite rotor blades have been investigated. To take into account the large deflections and rotations of rotor blades, a large-deflection beam model was used. A free-wake model based on vortex-lattice method was used to obtain the aerodynamic forces while considering wake effects. Newton–Raphson iteration method was applied to the aeroelastic analysis to obtain the numerical solutions. The flap, lag, and torsion deflections considering wake effects by using the free-wake model were investigated and compared with the results using two-dimensional quasi-steady model. Finally, aerodynamic changes after aeroelastic deflections were investigated.

Nomenclature

A_{cs}, B_{cs}, D_{cs}	=	cross-sectional stiffness matrices
$\tilde{e}_i^*$	=	local coordinates on the elastic axis after rotation and deformation
$G(q)$	=	gyroscopic matrix
K_A	=	tangential aerodynamic matrix
K_C	=	centrifugal stiffness matrix
K_T	=	tangential stiffness matrix
$M(q)$	=	mass matrix
$P(q)$	=	internal elastic force vector
$P_A(q)$	=	aerodynamic force vector
$P_C(q)$	=	centrifugal force vector
P_N	=	normal force on the elastic axis
P_S	=	tangential force on the elastic axis
q	=	generalized nodal displacement vector
$T(x_1)$	=	rotating transformation matrix

I. Introduction

MANY studies of helicopter rotor systems have been conducted over the past five decades. In general, high-aspect-ratio rotor blades are modeled as one-dimensional beams rather than three-dimensional structures because it allows a reduction in the computational time and effective results can still be achieved. In most of the earlier studies, linear beam models were adopted for helicopter rotor blades. However, it was revealed that the nonlinear behavior of the rotor blades affect the aeroelastic characteristics. Then the research focus altered to concentrate on the structural characteristics of the nonlinear beam models. There are two major nonlinear beam models. One is the moderate-deflection beam model that is based on ordering schemes to construct the transformation matrix. The moderate-deflection beam model has been applied to most rotor blade structural models [1–5]. However, in the case of the transformation matrix with high-order nonlinear terms, it is a difficult and complex process to construct the governing equations. In addition, as the nonlinearities of the rotor blades increase, the numerical error due to high-order nonlinear terms may increase [6]. The other nonlinear beam model is the large-deflection beam model that is not based on ordering schemes [7–11]. There are no artificial restrictions in the large-deflection beam model; it is assumed that the strain level remains low even if large deflections and rotations of the beam occur. It has been shown that the boundary of the aeroelastic stability could be changeable in the high-thrust state using the large-deflection beam model instead of the moderate-deflection beam model using ordering schemes [12,13].

Aerodynamic models should interact with the structural models in the aeroelastic model to investigate the aeroelastic characteristics. The quasi-steady theory, Greenberg's extension [14] of Theodorsen's theory, and Loewy's theory [15] have often been used for two-dimensional aerodynamic models. These theories use advantages that can reduce the computational time and simplify the aerodynamic models. However, these theories are limited when used to consider wake effects. To overcome this limitation, wake models have become popular in three-dimensional aerodynamic models. The prescribed wake model [16,17] is one of the most well-known wake models, and when used in an aeroelastic model, it can cause differences in the results compared with the two-dimensional aerodynamic models [18,19]. Aerodynamic characteristics can be investigated accurately for linear twist of the blade using the prescribed wake model. However, it is difficult to apply the prescribed wake model in the aeroelastic model if there are strong wake effects or if the blade twist is nonlinear [20,21]. To overcome these limitations, the free-wake model has been applied to the aerodynamic models [22–24]. In particular, since 2000, the free-wake model has been used to investigate aeroelastic characteristics [25,26].

In most of the above-mentioned studies, two-dimensional aerodynamic models with restricted wake effects were used in the aeroelastic models. The wake models were mentioned in several studies, but most studies were on rigid blades without aeroelastic deflections. In this paper, the aeroelastic deflections for isotropic and composite rotor blades in hover have been investigated. To consider the nonlinear behavior of the blades, a large-deflection beam model was applied to the structural model. In addition, the free-wake model based on the vortex-lattice method (VLM) used to generate unsteady wakes and to calculate the aerodynamic loadings was applied to the aerodynamic model. The aerodynamic characteristics, after the aeroelastic deflections, have also been investigated.

II. Method

A. Structural Modeling for a Rotating Blade

The high-aspect-ratio rotor blades undergo large deflections and rotations. In general, a rotating blade is considered as a one-dimensional beam. In particular, a composite blade is considered as a box beam. A rotating blade with this consideration is shown in Fig. 1.

Received 7 July 2010; revision received 15 March 2011; accepted for publication 28 March 2011.

*Graduate Research Assistant, School of Mechanical Aerospace and Systems Engineering, Division of Aerospace Engineering, 335 Gwahangno, Yuseong-gu, Daejeon, Korea.

†Professor, School of Mechanical Aerospace and Systems Engineering, Division of Aerospace Engineering, 335 Gwahangno, Yuseong-gu. Fellow AIAA.

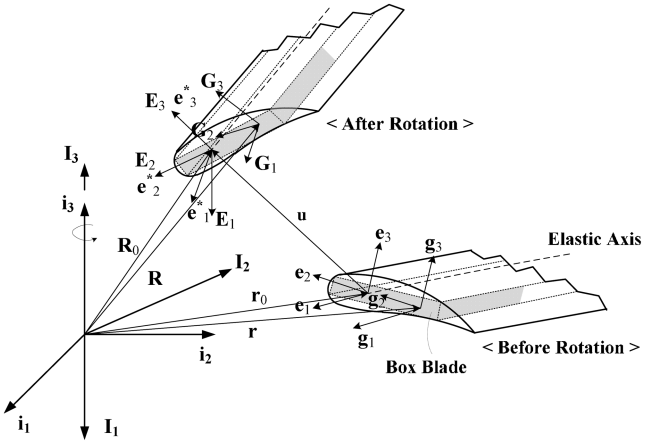

Fig. 1 Blade before and after rotation induced by deformation.

In Fig. 1, $\mathbf{e}_1^*$, $\mathbf{e}_2^*$, and $\mathbf{e}_3^*$ refer to the local coordinates on the elastic axis after rotation and have the following relationship:

$$\mathbf{e}_i^* = T(x_1)\mathbf{i}_i \tag{1}$$

where $T(x_1)$ is the rotating transformation matrix, as follows:

$$T(x_1) = \begin{bmatrix} \cos\beta\cos\psi & \cos\beta\sin\psi & \sin\beta \\ -\sin\theta\sin\beta\cos\psi & -\sin\theta\sin\beta\sin\psi + \cos\theta\cos\psi & \sin\theta\cos\beta \\ -\cos\theta\sin\beta\cos\psi & -\cos\theta\sin\beta\sin\psi - \sin\theta\cos\psi & \cos\theta\cos\beta \end{bmatrix} \tag{2}$$

$$\psi = \psi_s + \psi_e \qquad \beta = \beta_{pc} + \beta_e \qquad \theta = \theta_p + \theta_e \tag{3}$$

where ψ_s is the sweep angle, ψ_e is the elastic lead-lag angle, β_{pc} is the precone angle, β_e is the elastic flap angle, θ_p is the collective pitch angle, and θ_e is the elastic twist angle.

The variations of the kinetic and strain energies for a rotating cantilever beam with a rotation speed of Ω are defined as follows:

$$\delta T = \int_0^l \int_A \rho\{\delta V\}^T\{V\}\,\mathrm{d}A\,\mathrm{d}x_1 \tag{4}$$

$$\delta U = \int_0^l \begin{Bmatrix} \delta\bar{e} \\ \delta\bar{\kappa} \end{Bmatrix}^T \begin{bmatrix} A_{\text{cs}} & B_{\text{cs}} \\ B_{\text{cs}}^T & D_{\text{cs}} \end{bmatrix} \begin{Bmatrix} \bar{e} \\ \bar{\kappa} \end{Bmatrix} \mathrm{d}x_1 \tag{5}$$

where the velocity vector $\{V\}$ is defined by both the elastic velocity of the blade on the rotating coordinates and the rotational velocity of the coordinate system. In addition, $\{\delta\bar{e}\}$ and $\{\delta\kappa\}$ represent axial and shearing strains and twist and bending strains at the elastic axis [12], respectively, and A_{cs}, B_{cs}, and D_{cs} are 3×3 cross-sectional stiffness matrices of the beam [13].

B. Aerodynamic Modeling Based on the Free-Wake Method

Unsteady wake is generated by rotating blades, and the flowfield around the rotors is extremely complicated and unstable. The rotor blades are subjected to a severe vibratory environment, due to the complicated and unstable flowfield in prolonged hovering flight. Therefore, the wake effects should be considered as key in calculating aerodynamic forces for aeroelastic analysis. In this paper, the free-wake method based on the VLM was applied to calculate the aerodynamic forces. The movable velocities of the wake in hover are the sum of the velocities due to the blade motions and the induced velocity from the wake; thus, the wake position can be determined by [22]

$$(\Delta x, \Delta y, \Delta z) = (u(t) + u_w, v(t) + v_w, w(t) + w_w)\Delta t \tag{6}$$

where each velocity is calculated using the Biot–Savart law. Using the unsteady Bernoulli's equation, the pressure difference of the blade is calculated as follows:

$$\begin{aligned} \Delta p_{ij} = \rho\Bigg\{ & [\mathbf{u}(t) + \mathbf{u}_w, \mathbf{v}(t) + \mathbf{v}_w, \mathbf{w}(t) + \mathbf{w}_w]_{ij} \\ & \cdot \boldsymbol{\tau}_i \frac{\Gamma_{i,j} - \Gamma_{i-1,j}}{\Delta c_{ij}} + [\mathbf{u}(t) + \mathbf{u}_w, \mathbf{v}(t) + \mathbf{v}_w, \mathbf{w}(t) + \mathbf{w}_w]_{ij} \\ & \cdot \boldsymbol{\tau}_j \frac{\Gamma_{i,j} - \Gamma_{i,j-1}}{\Delta b_{ij}} + \frac{\partial}{\partial t}\Gamma_{ij} \Bigg\} \end{aligned} \tag{7}$$

Then the lift and pitch moment coefficients are defined as follows:

$$c_l(x_1, t) = \frac{-(\Delta p \Delta S)_{ij}\hat{n}_{ij}}{\frac{1}{2}\rho_a U^2 c} \tag{8}$$

$$c_m(x_1, t) = \frac{-(\Delta p \Delta S)_{ij}x_{2i}}{\frac{1}{2}\rho_a U^2 c^2} \tag{9}$$

where ΔS is the area of the vortex lattices, and x_{2i} is the distance between the elastic axis and the collocation points of the vortex lattices. The aerodynamic loadings calculated using the free-wake method based on the VLM are shown in Fig. 2. The aspect ratio of the blade is about 5.2, the radius of the rotor is 91.5 in., and rotation speed is 496 fps. The results were compared with experiments [27]. In this case, the blade is sufficiently rigid to ignore the elastic deflections. Thus, the structural characteristics were not considered. Figure 2 shows the numerical and experimental [27] results in excellent agreement. In the case of the pitching moment at the aerodynamic center, it should theoretically be zero for the symmetric airfoil. However, as shown in Fig. 3, it was not exactly zero, even though the pressure distributions in Fig. 4 were in good agreement with experiments [27]. Thus, the pitching moment in the aeroelastic analysis can affect the aeroelastic deflections. On the other hand, the aerodynamic forces were applied to the aeroelastic model to predict the aeroelastic deflections after 10 revolutions, in alignment with the results of the convergence in Fig. 5. The wake configurations obtained in this research are shown in Fig. 6.

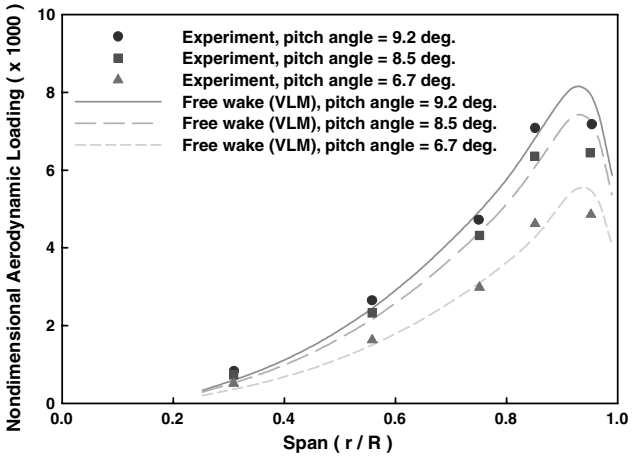

Fig. 2 Comparisons of aerodynamic loadings.

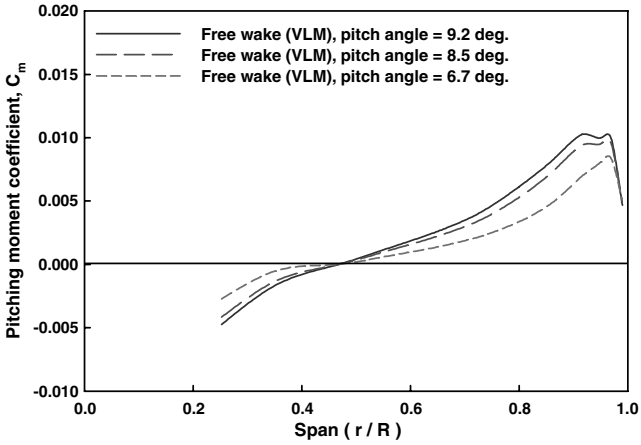

Fig. 3 Pitching moment coefficients.

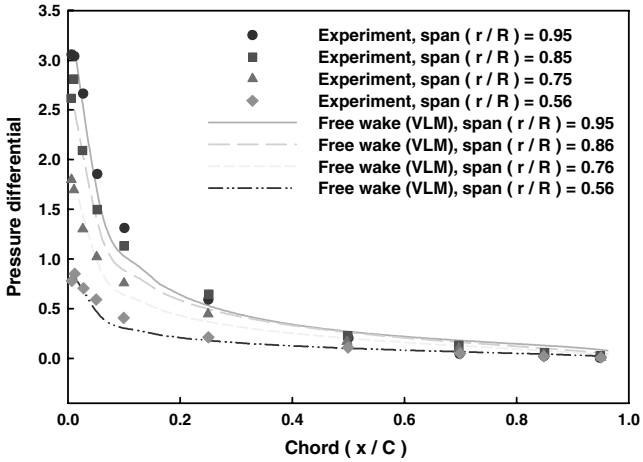

Fig. 4 Chordwise pressure distributions (pitch angle is 8.5 deg).

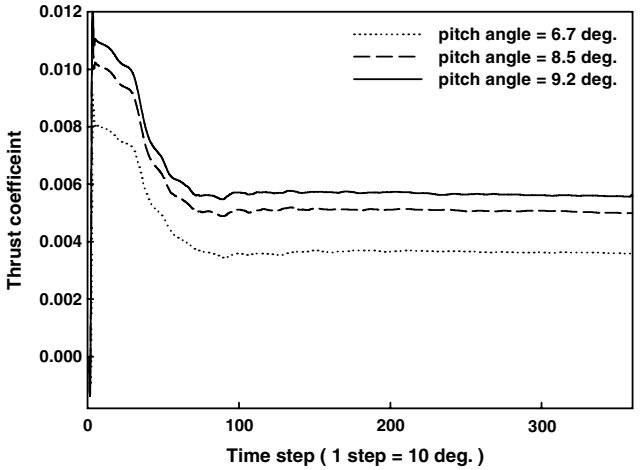

Fig. 5 Convergence of thrust coefficient.

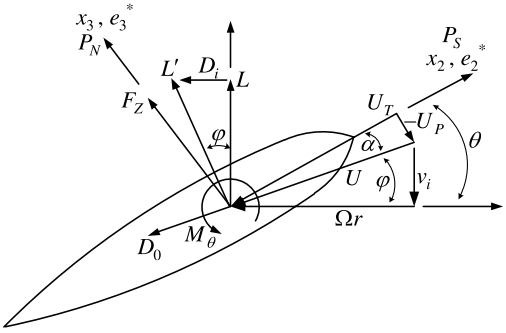

Fig. 7 External force and moment on the elastic axis.

The virtual work done by the external forces can be expressed as follows:

$$\delta W = \int_0^l \int_A \{\delta \mathbf{R}\}^T \{\mathbf{f}\}\, \mathrm{d}A\, \mathrm{d}x_1 \tag{10}$$

In Eq. (10), $\{\bar{f}\}$ consists of external forces and moment such as P_S, P_N, and M_θ. Then the tangential and normal forces shown in Fig. 7, which represent the external forces on the elastic axis, are defined using the obtained aerodynamic force as follows:

$$P_S = L' \sin\alpha - D_0 \cos\alpha \tag{11}$$

$$P_N = L' \cos\alpha + D_0 \sin\alpha \tag{12}$$

where α indicates the effective angle of attack and D_0 is the initial profile drag. Then Eq. (10) can be rewritten as follows:

$$\delta W = \int_0^l \begin{Bmatrix} \delta u \\ \delta\alpha \end{Bmatrix}^T \begin{bmatrix} T^T & 0 \\ 0 & C_{K1}^T \end{bmatrix} \begin{Bmatrix} N_a \\ M_a \end{Bmatrix} \mathrm{d}x_1 \tag{13}$$

$$\{N_a\} = \begin{Bmatrix} 0 \\ P_S \\ P_N \end{Bmatrix}, \qquad \{M_a\} = \begin{Bmatrix} M_\theta \\ 0 \\ 0 \end{Bmatrix} \tag{14}$$

In addition, Eq. (13) is rewritten as a form of the finite element term:

$$P_A(q) = \int_0^l H^T \begin{bmatrix} T^T & 0 \\ 0 & C_{K1}^T \end{bmatrix} \begin{Bmatrix} N_a \\ M_a \end{Bmatrix} \mathrm{d}x_1 \tag{15}$$

$$\begin{Bmatrix} u \\ \alpha \end{Bmatrix} = H\{q\} \tag{16}$$

where H is the shape-function matrix.

C. Aeroelastic Deflections

The finite element governing equation for aeroelastic analysis, defined by using kinetic energy, strain energy, and virtual work in the Hamilton's extended principle, is

$$\frac{1}{\Omega^2} M(q)\{\ddot{q}\} + \frac{1}{\Omega} G(q)\{\dot{q}\} + P(q) - P_C(q) = P_A(q) \tag{17}$$

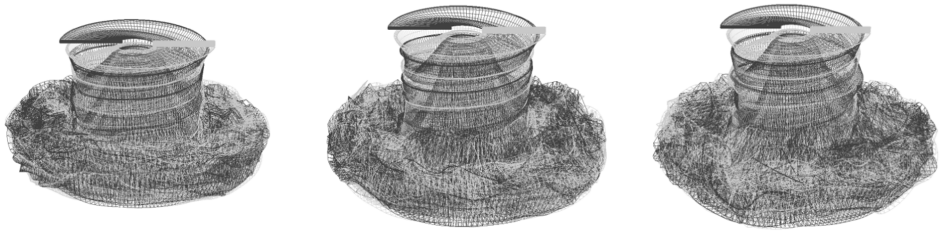

a) Pitch angle = 6.7 deg **b) Pitch angle = 8.5 deg** **c) Pitch angle = 9.2 deg**

Fig. 6 Wake configurations after 10 revolutions for a two-bladed rotor.

where $M(q)$ is the mass matrix, $G(q)$ is the gyroscopic matrix, $P(q)$ is the internal elastic force vector, $P_C(q)$ is the centrifugal load vector, and $P_A(q)$ is the converged steady aerodynamic force vector. In addition, q is the generalized nodal displacement vector, which consists of three translational and three rotational degrees of freedom, and Ω is the angular velocity of the blade. By assuming an equilibrium state for the equilibrium deflections, Eq. (17) can be simplified by ignoring the time-dependent terms as follows:

$$f(q) = P(q) - P_C(q) - P_A(q) = 0 \tag{18}$$

Equation (18) can be rewritten as a form of stiffness and force by applying the Taylor series extension:

$$[K_T^{(i-1)} - K_C^{(i-1)} - K_A^{(i-1)}]\{\Delta q^{(i)}\} = P_C(q^{(i-1)}) - P(q^{(i-1)}) + P_A(q^{(i-1)}) \tag{19}$$

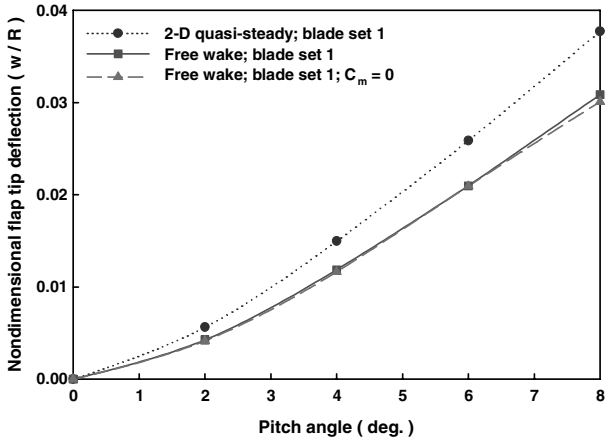

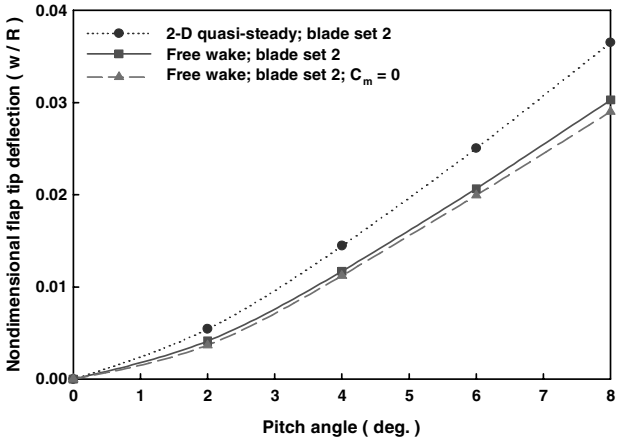

a) Flap tip deflection

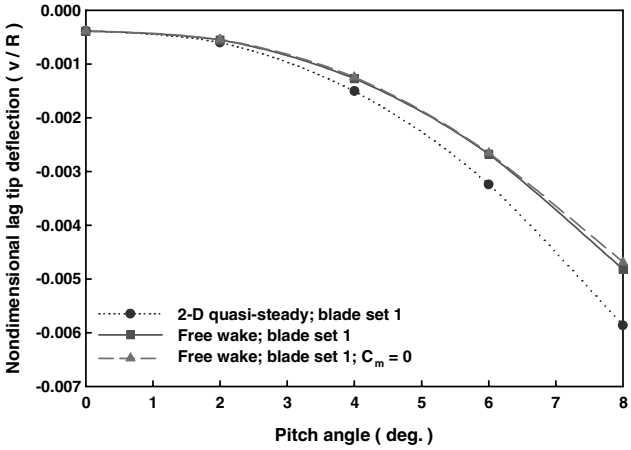

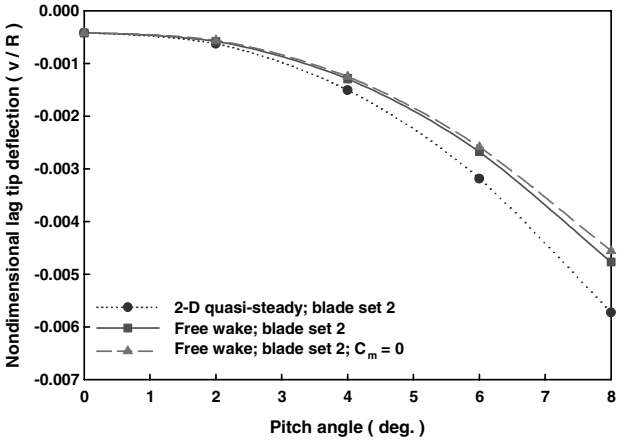

b) Lag tip deflection

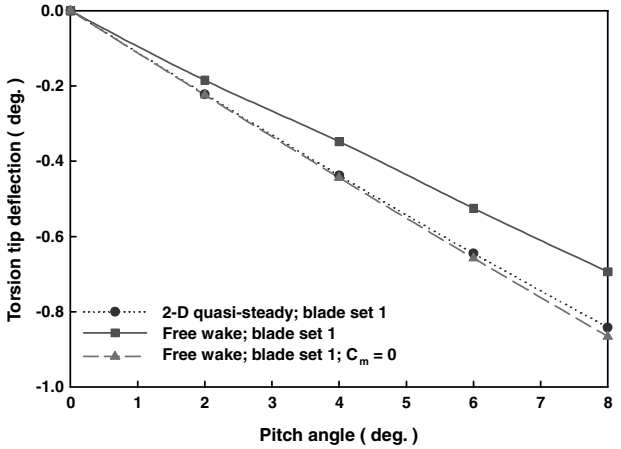

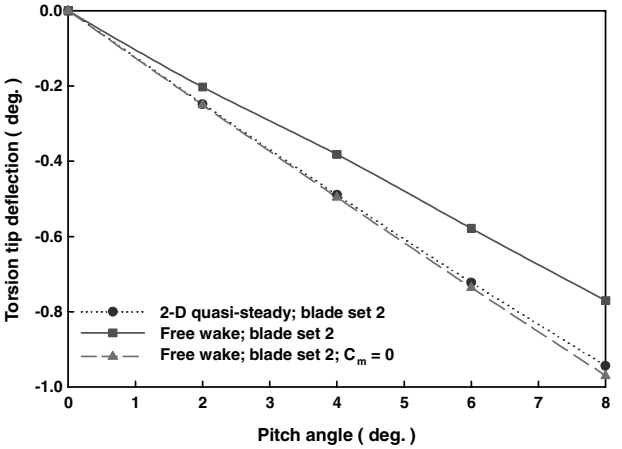

c) Torsion tip deflection

Fig. 8 Aeroelastic tip deflections versus increasing pitch angles.

where $K_T^{(i-1)} = (\partial P/\partial q)|_{q^{(i-1)}}$ is the tangential stiffness matrix, $K_C^{(i-1)} = (\partial P_C/\partial q)|_{q^{(i-1)}}$ is the centrifugal stiffness matrix, and $K_A^{(i-1)} = (\partial P_A/\partial q)|_{q^{(i-1)}}$ is the tangential aerodynamic matrix. Finally, the equilibrium deflection $q_0 = q^{(i)}$ is obtained by applying the Newton–Raphson method, as shown in Eq. (19).

III. Analysis Results and Discussion

A. Isotropic Rotor Blade

The flap, lag, and torsion tip deflections, as functions of pitch angles, are shown in Fig. 8, and deflections at a pitch angle of 8 deg along the span direction are shown in Fig. 9. The rotor model is a

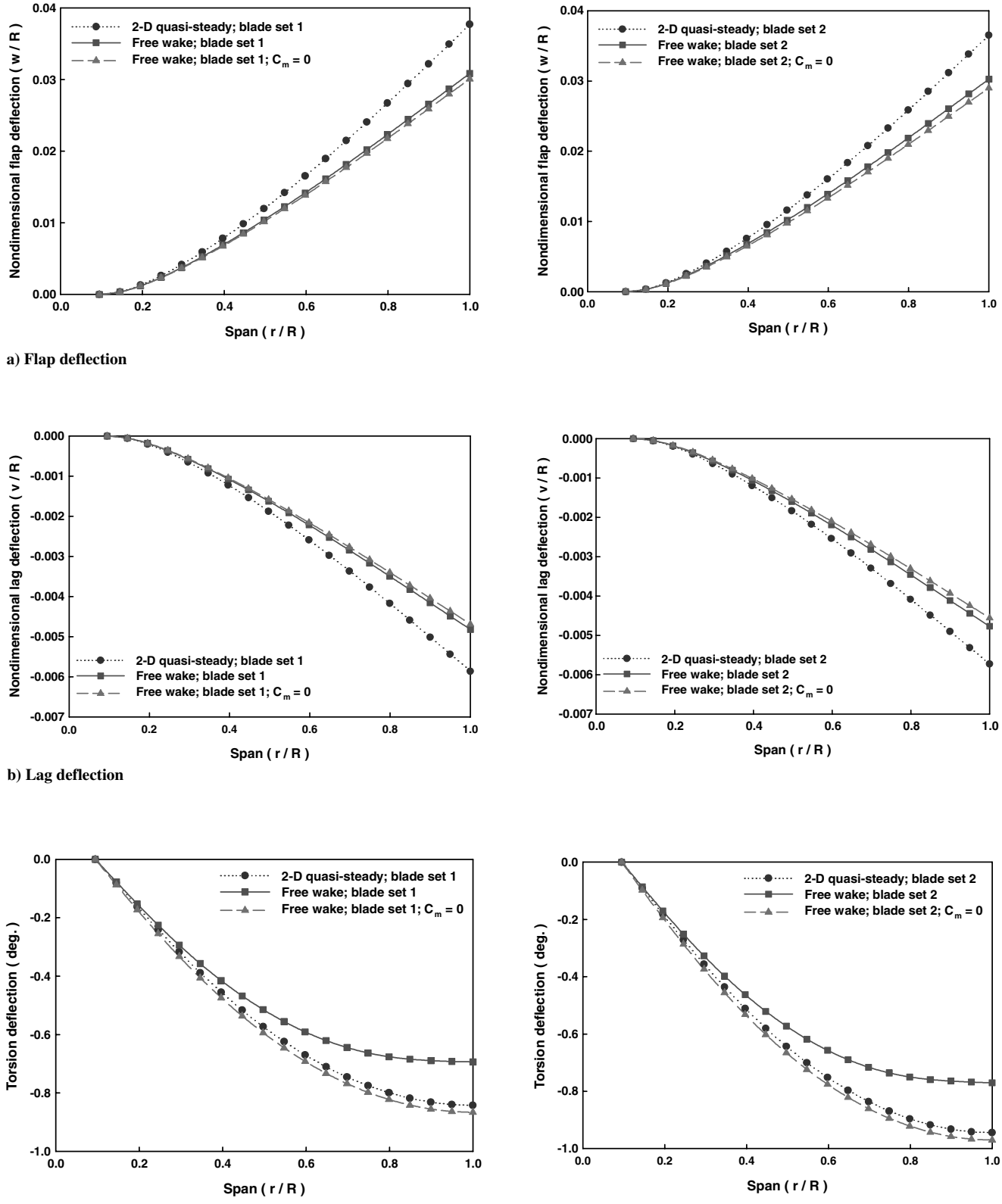

a) Flap deflection

b) Lag deflection

c) Torsion deflection

Fig. 9 Spanwise aeroelastic deflections (pitch angle is 8 deg).

Table 1 Blade stiffness properties [28]

Parameters	Symbol	Units	Set 1	Set 2
Chordwise center of gravity	——	%	24.9	24.8
Elastic axis	——	%	25.4	24.8
Flap bending stiffness	EI_β	N-m^2	17.37	17.22
Chord bending stiffness	EI_ζ	N-m^2	407.7	357.8
Torsional rigidity	GJ	N-m^2	6.32	5.10

Table 2 Rotor parameter values [28]

	Isotropic blade	
Parameter	Set 1	Set 2
Rotor speed Ω, rpm	1000	1000
Airfoil section lift-curve slope a_0	2π	2π
Profile drag coefficient C_{d0}	0.0079	0.0079
Hub offset ratio	0.1051	0.1051
Nonrotating lead-lag structural damping	0.00826	0.007423
Lock number γ	5.115	5.042
k_m, k_{m2}, kg · m	1.911×10^{-4}	1.744×10^{-4}
k_{m1}, kg · m	0	0

two-bladed system with a radius of 0.9615 m and a chord length of 0.0864 m. The blade stiffness properties and rotor parameter values are described in Tables 1 and 2 [28]. The results using the free-wake method were compared with the results of the two-dimensional quasi-steady model referred to in [12]. In most cases, the deflections increased as the pitch angle increased. There are several important characteristics of the deflections. One is that the flap and lag deflections using the free-wake method were smaller than the results using two-dimensional quasi-steady model. It is well known that aerodynamics at the tip of the blade are generally decreased, due to the tip vortex. That is called the tip-loss effect. In the two-dimensional quasi-steady model, the tip-loss effect cannot be considered by itself. The tip-loss factor should be added. On the other hand, the tip-loss effect can be implicitly considered by applying the free-wake method (see Fig. 2). To conclude, the tip-loss effect caused the differences of flap and lag deflections. Secondarily, in the cases of the torsion deflections, the results were altered by the pitching moments. In general, the pitching moment of a symmetric airfoil at the quarter-chord aerodynamic center is regarded as zero. In this sense, the pitching moment at the quarter-chord aerodynamic center with a thin-airfoil assumption can be assumed to be zero. The torsion deflections using the free-wake method were similar to the results using a two-dimensional quasi-steady model when the pitching moments for both aerodynamic models were assumed to be zero. In this case, the torsion deflections were only affected by the torsional rigidity in Table 1. In contrast, the torsion deflections using the free-wake method without any restrictions were smaller than the results using two-dimensional quasi-steady model. The pitching moments using free-wake method without any restrictions were not exactly zero, due to the unsteady returning wakes (see Fig. 10), and the nonzero pitching moments led to the differences of the torsion deflections. Finally, the other important characteristic of aeroelastic deflections is that the torsion deflection appeared in the negative region. This factor led to a decrease in the aerodynamic lift because negative torsion deflection resulted in the decrease of the effective angle of attack. The aerodynamic changes after aeroelastic deflections at a pitch angle of 8 deg are shown in Fig. 10.

B. Composite Rotor Blade

To analyze the composite rotor blades, it is necessary to obtain the cross-sectional stiffness matrices, A_{cs}, B_{cs}, and D_{cs}. The configuration of a composite box beam is shown in Fig. 11. The composite material properties and rotor parameters are shown in Table 3. The cross-sectional stiffness matrices were calculated by referring to [13]; the calculated meaningful values are shown in Table 4.

The flap, lag, and torsion tip deflections, as functions of pitch angles, are shown in Fig. 12, and the deflections at a pitch angle of 10 deg along the span direction are shown in Fig. 13. The rotor is a two-bladed system. Most tendencies of the deflections were similar to those of the isotropic blade. The flap and lag deflections using the free-wake method were smaller than the results using the two-dimensional quasi-steady model, due to the tip-loss effect, and the deflections differed, due to the different cross-sectional stiffnesses induced by the different fiber angles. For the composite blade, the torsion deflection was more affected by composite coupling effects than by wake effects. The torsion deflections using the free-wake method were similar to the results using two-dimensional quasi-steady model, regardless of the nonzero pitching moment. In addition, the torsion deflection appeared in the positive region for -20 deg of θ_f, but appeared in the negative region for 0 and 90 deg. The flap bending–twist coupling effect in Table 4 caused the different tendency of the torsion deflection. Moreover, this fact led to an

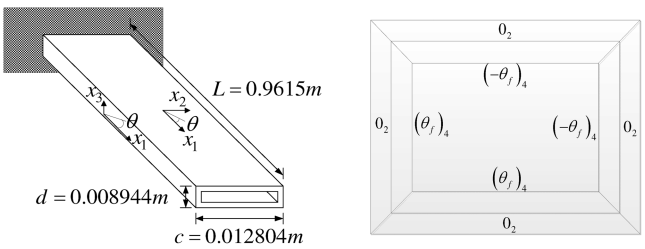

Fig. 11 Configuration of composite box beam.

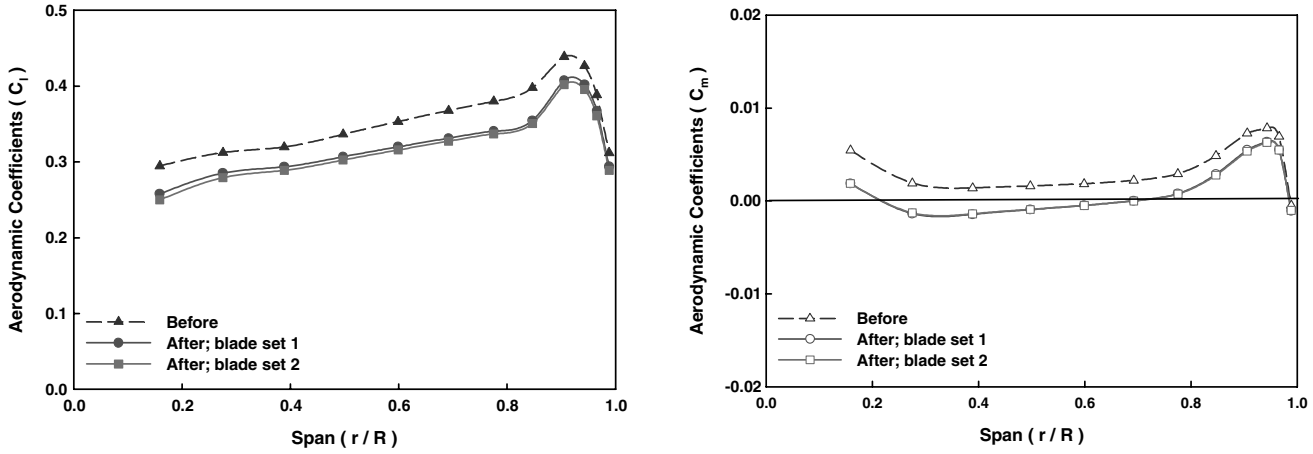

a) Lift coefficient **b) Pitching moment coefficient**

Fig. 10 Aerodynamic changes before and after aeroelastic deflections (pitch angle is 8 deg).

Table 3 Composite material properties and rotor parameters

AS4/3501-6 graphite/epoxy		Rotors	
Parameter	Value	Parameter	Value
E_1, GPa	142	Rotor speed Ω, rpm	1000
E_2, GPa	9.81	Airfoil section lift-curve slope a_0	2π
G_{12}, GPa	6.0	Profile drag coefficient C_{d0}	0.0079
G_{23}, GPa	3.77	Lock number γ	5.593
ν_{12}	0.3	k_m, k_{m2}, kg · m	2.062×10^{-4}
ν_{23}	0.34	k_{m1}, kg · m	0

Table 4 Cross-sectional stiffness

θ_f, deg	Flap bending–twist D_{12}, Nm^2	Lag bending–twist D_{13}, Nm^2	Extension-twist B_{11}. Nm
−20	-1.356×10^{-2}	0	-3.002×10^{3}
0	0	0	0
90	0	0	4.948

increase in the aerodynamic lift for −20 deg of θ_f, but decrease for 0 and 90 deg (see Fig. 14).

IV. Conclusions

Aeroelastic deflections and aerodynamic changes considering wake effects of hovering rotors have been investigated. To take into account the large deflections and rotations of rotor blades, a large-deflection beam model was used. In addition, the free-wake model, based on the vortex-lattice method, was used to obtain the aerodynamic forces while considering wake effects.

The flap and lag deflections considering wake effects including the tip-loss effect by using the free-wake model were predicted smaller than the results using two-dimensional quasi-steady model. In the case of the pitching moment, it is regarded as zero for a symmetric airfoil at the quarter-chord aerodynamic center. In this sense, the

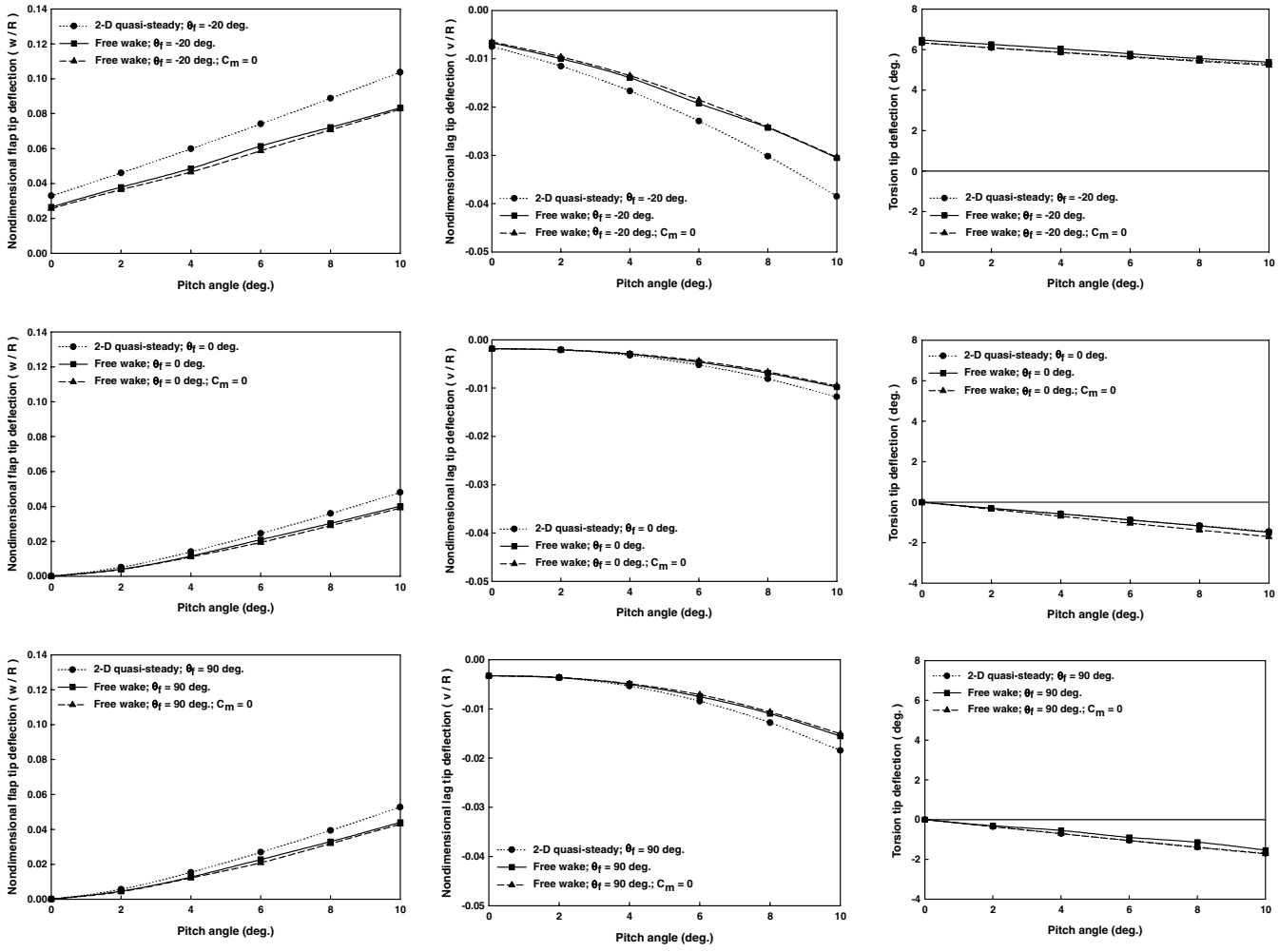

a) Flap tip deflection **b) Lag tip deflection** **c) Torsion tip deflection**

Fig. 12 Aeroelastic tip deflections versus increasing pitch angles.

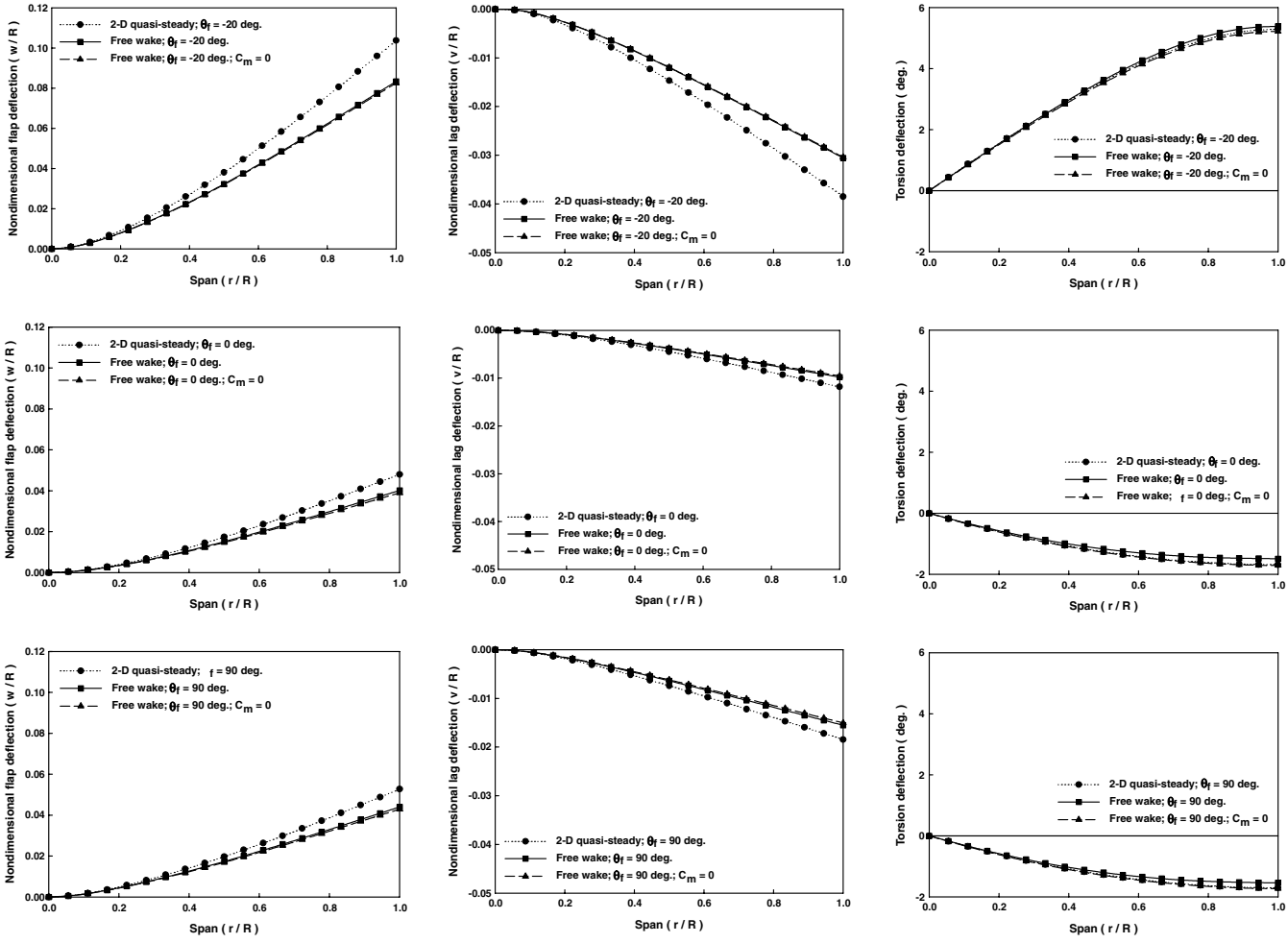

a) Flap deflection **b) Lag deflection** **c) Torsion deflection**

Fig. 13 Aeroelastic deflections along the spanwise direction (pitch angle is 10 deg).

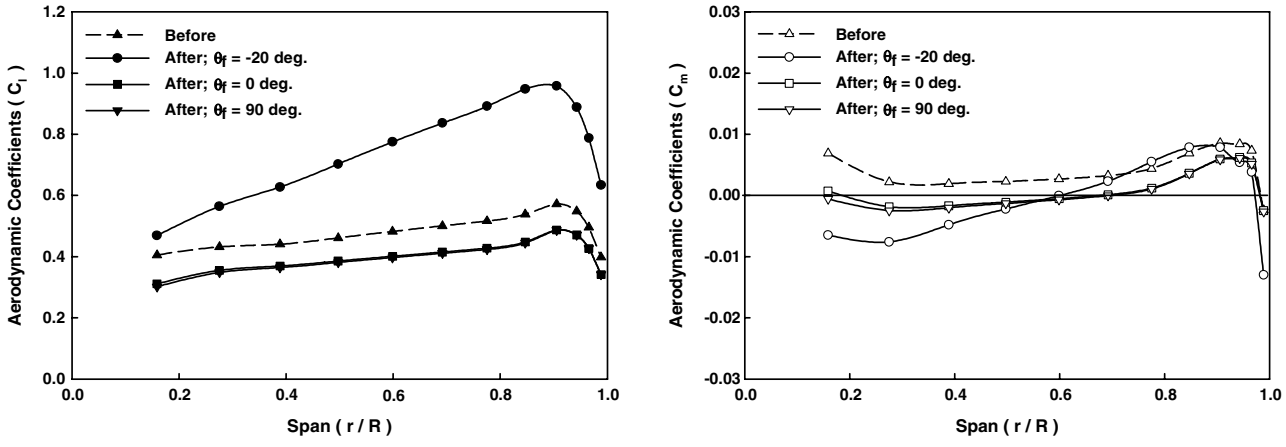

a) Lift coefficient **b) Pitching moment coefficient**

Fig. 14 Aerodynamic changes before and after the aeroelastic deflections (pitch angle is 10 deg).

pitching moment at the quarter-chord aerodynamic center with a thin-airfoil assumption can be assumed to be zero. However, the pitching moments using free-wake method without any restrictions were not exactly zero, due to the unsteady returning wakes. The nonzero pitching moment affected the torsion deflection, but not the flap and lag deflections. In the cases of the composite rotor blades, composite coupling effects (rather than the nonzero pitching moment), especially the bending–twist coupling effect, significantly affected the torsion deflection. Finally, the lift distributions after the aeroelastic deflections were differently investigated and were compared with the results before the aeroelastic deflections. The lift increased when the torsion deflection appeared in the positive region. On the contrary, the lift decreased when the torsion deflection appeared in the negative region. In the final analysis, it was shown that the wake effects are significant for an accurate estimation of the rotor performance.

Acknowledgments

This research was supported by World Class University program through the National Research Foundation of Korea funded by the Ministry of Education, Science, and Technology, and by Korea Aerospace Research Institute under Aerospace Parts Technology Research Program (Aeroelastic Analysis of Bearingless Rotor System) funded by the Ministry of Knowledge Economy.

References

[1] Hodges, D. H., and Dowell, E. H., "Nonlinear Equations of Motion for Elastic Bending and Torsion of Twisted Non-uniform Rotor Blades," NASA TN D-7818, 1974.

[2] Rosen, A., and Friedmann, P. P., "Nonlinear Elastic Equations of Equilibrium for Elastic Helicopter or Wind Turbine Blades Undergoing Moderate Deformation," NASA CR-159478, 1978.

[3] Rosen, A., and Friedmann, P. P., "The Nonlinear Behavior of Elastic Slender Straight Beams Undergoing Small Strains and Moderate Rotations," *Journal of Applied Mechanics*, Vol. 46, No. 1, March 1979, pp. 161–168. doi:10.1115/1.3424490

[4] Chandra, R., Stemple, A. D., and Chopra, I., "Thin-Walled Composite Beams Under Bending, Torsion, and Extensional Loads," *Journal of Aircraft*, Vol. 27, No. 7, 1990, pp. 619–626. doi:10.2514/3.25331

[5] Chandra, R., and Chopra, I., "Experimental and Theoretical Investigation of the Vibration Characteristics of Rotating Composite Box Beams," *Journal of Aircraft*, Vol. 29, No. 4, 1992, pp. 657–664. doi:10.2514/3.46216

[6] Panda, B., "Assembly of Moderate-Rotation Finite Elements Used in Helicopter Rotor Dynamics," *Journal of the American Helicopter Society*, Vol. 32, No. 4, Oct. 1987, pp. 63–69. doi:10.4050/JAHS.32.63

[7] Hodges, D. H., "Nonlinear Equations for the Dynamics of Pretwisted Beams Undergoing Small Strains and Large Rotations," NASA TP-2470, 1985.

[8] Danielson, D. A., and Hodges, D. H., "A Beam Theory for Large Global Rotation, Moderate Local Rotation, and Small Strain," *Journal of Applied Mechanics*, Vol. 55, 1988, pp. 179–184. doi:10.1115/1.3173625

[9] Bauchau, O. A., and Hong, C. H., "Finite Element Approach to Rotor Blade Modeling," *Journal of the American Helicopter Society*, Vol. 32, No. 1, 1987, pp. 60–67. doi:10.4050/JAHS.32.60

[10] Hodges, D. H., Hopkins, A. S., Kunz, D. L., and Hinnant, H. E., "Introduction to GRASP—General Rotorcraft Aeromechanical Stability Program—A Modern Approach to Rotorcraft Modeling," *Journal of the American Helicopter Society*, Vol. 32, No. 2, 1987, pp. 78–90. doi:10.4050/JAHS.32.78

[11] Bauchau, O. A., and Hong, C. H., "Nonlinear Composite Beam Theory," *Journal of Applied Mechanics*, Vol. 55, 1988, pp. 156–163. doi:10.1115/1.3173622

[12] Cho, M. H., and Lee, I., "Aeroelastic Stability of Hingeless Rotor Blade in Hover Using Large Deflection Theory," *AIAA Journal*, Vol. 32, No. 7, 1994, pp. 1472–1477. doi:10.2514/3.12217

[13] Jeon, S. M., Cho, M. H., and Lee, I., "Aeroelastic Analysis of Composite Rotor Blades in Hover," *Computers and Structures*, Vol. 66, No. 1, 1998, pp. 59–67. doi:10.1016/S0045-7949(97)00057-6

[14] Greenberg, J. M., "Airfoil in Sinusoidal Motion in a Pulsating Stream," NACA TN-1326, June 1947.

[15] Loewy, R. G., "A Two-Dimensional Approximation to the Unsteady Aerodynamics of Rotary Wings," *Journal of the Aeronautical Sciences*, Vol. 24, No. 2, 1957, pp. 81–92.

[16] Landgrebe, A. J., "The Wake Geometry of a Hovering Helicopter Rotor and Its Influence on Rotor Performance," *Journal of the American Helicopter Society*, Vol. 17, No. 4, Oct. 1972, pp. 3–15. doi:10.4050/JAHS.17.3

[17] Kocurek, J. D., and Tangler, J. L., "A Prescribed Wake Lifting Surface Hover Performance Analysis," *Journal of the American Helicopter Society*, Vol. 22, No. 1, Jan. 1977, pp. 24–35. doi:10.4050/JAHS.22.24

[18] Yoo, K. M., "Unsteady Vortex Lattice Aerodynamics for Rotor Aeroelasticity in Hover and in Forward Flight," Ph.D. Thesis, Georgia Institute of Technology, 1989.

[19] Kwon, O. J., Hodges, D. H., and Sankar, L. N., "Stability of Hingeless Rotors in Hover Using Three-Dimensional Unsteady Aerodynamics," *Journal of the American Helicopter Society*, Vol. 36, No. 2, Apr. 1991, pp. 21–31. doi:10.4050/JAHS.36.21

[20] Müller, R. H. G., "Special Vortices at a Helicopter Rotor Blade," *Journal of the American Helicopter Society*, Vol. 35, No. 4, October 1990, pp. 16–21. doi:10.4050/JAHS.35.16

[21] Kim, J. M., Komerath, N. M., and Liou, S. G., "Vorticity Concentration at the Edge of the Inboard Vortex Sheet," *Journal of the American Helicopter Society*, Vol. 39, No. 2, April 1994, pp. 30–34. doi:10.4050/JAHS.39.30

[22] Na, S. U., "Development of a Time-Marching Free-Wake Method for the Prediction of Helicopter Rotor Wake Geometry and Performance," Ph.D. Thesis, Korea Advanced Institute of Science and Technology, Daejeon, ROK, 1998.

[23] Clark, D. R., and Leiper, A. C., "The Free Wake Analysis; A Method for the Prediction of Helicopter Rotor Hovering Performance," *The 25th Annual National Forum of the American Helicopter Society*, AHS International, Alexandria, VA, May 1969.

[24] Miller, R. H., "Rotor Hovering Performance Using the Method of Fast Free Wake Analysis," *Journal of Aircraft*, Vol. 20, No. 3, 1983, pp. 257–261. doi:10.2514/3.44861

[25] Cribbs, R. C., Friedmann, P. P., and Chiu, T., "Coupled Helicopter Rotor/Flexible Fuselage Aeroelastic Model for Control of Structural Response," *AIAA Journal*, Vol. 38, No. 10, 2000, pp. 1777–1788. doi:10.2514/2.838

[26] Theodore, C., and Celi, R., "Helicopter Flight Dynamic Simulation with Refined Aerodynamics and Flexible Blade Modeling," *Journal of Aircraft*, Vol. 39, No. 4, 2002, pp. 577–586. doi:10.2514/2.2995

[27] John, P. R., "Static-Thrust Measurements of the Aerodynamic Loading on a Helicopter Rotor Blade," NACA TN 3688, 1956.

[28] Sharpe, D. L., "An Experimental Investigation of the Flap-Lag-Torsion Aeroelastic Stability of a Small-Scale Hingeless Helicopter Rotor in Hover," NASA Technical Paper 2546, Jan. 1986.